

# Sulfur-Doped Nanographenes Containing Multiple Subhelicenes

Wenhui Niu, Yubin Fu, Hartmut Komber, Ji Ma, Xinliang Feng, Yiyong Mai,\* and Junzhi Liu\*

Cite This: *Org. Lett.* 2021, 23, 2069–2073

Read Online

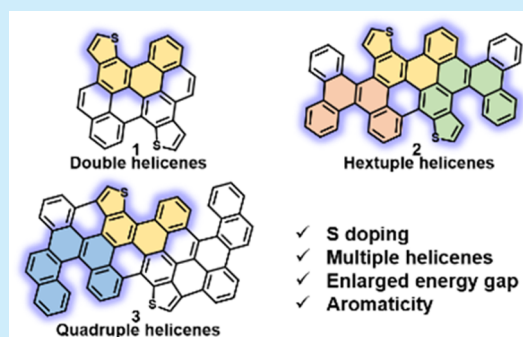
ACCESS |

Metrics & More

Article Recommendations

Supporting Information

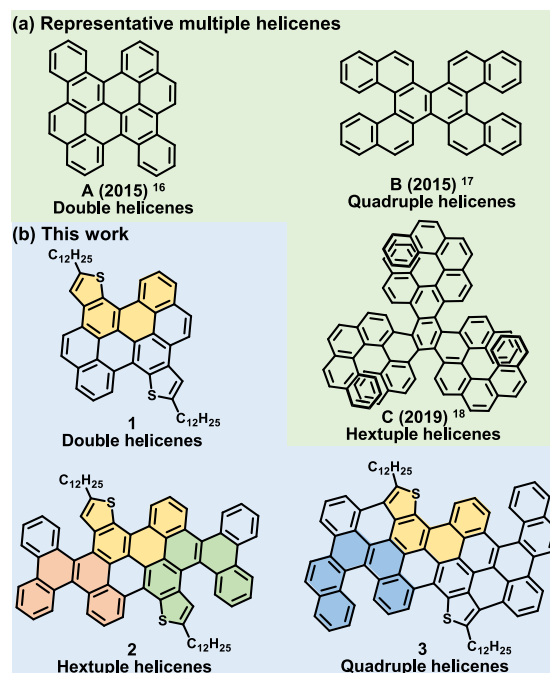
**ABSTRACT:** In this work, we describe the synthesis and characterization of three novel sulfur-doped nanographenes (NGs) (1–3) containing multiple subhelicenes, including carbo[4]helicenes, thieno[4]helicenes, carbo[5]helicenes, and thieno[5]helicenes. Density functional theory calculations reveal that the helicene substructures in 1–3 possess dihedral angles from 15° to 34°. The optical energy gaps of 1–3 are estimated to be 2.67, 2.45, and 2.30 eV, respectively. These three sulfur-doped NGs show enlarged energy gaps compared to those of their pristine carbon analogues.



As an important class of nanographenes (NGs), nonplanar NGs adopt curved structures either by embedding nonhexagonal rings<sup>1,2</sup> or by introducing steric strain from atom crowding,<sup>3</sup> such as [4]helicene (cove-edged structure), [5]helicene (fjord-edged structure), and even higher helicenes.<sup>4–6</sup> Benefiting from the curvature, nonplanar NGs bearing helical substructures exhibit enhanced solubility compared to those of their planar counterparts, which enable the promising applications in organic field-effect transistors (OFETs),<sup>3</sup> chiral-induced spin selectivity,<sup>7</sup> molecular recognition and machines, etc.<sup>8–10</sup> Apart from a number of examples of nonplanar NGs containing a single-helicene substructure,<sup>11–15</sup> considerable progress has been made in multiple subhelicenes, which showed highly distorted geometry by accumulation of helical repulsion, as exemplified by A–C<sup>16–18</sup> (Figure 1a). Upon incorporation of multiple helicene substructures, those nonplanar NGs may not only exhibit richer three-dimensional geometry, more possible diastereomers, and dynamics of isomerization but also display unique molecular packing motifs,<sup>19,20</sup> which favor their charge carrier transport in electronic devices.<sup>3</sup>

Compared to their pristine carbon analogues, NGs doped with heteroatoms such as nitrogen, sulfur, and boron in the aromatic skeleton have been shown to exhibit tailored optoelectronic properties.<sup>21–25</sup> Among them, sulfur-doped NGs have attracted growing interest in the past decade,<sup>26–28</sup> due to their highly localized electronic structures contributed by the electron richness and polarizability of sulfur atoms. However, the sulfur-doped NGs with multiple subhelicenes have received limited attention,<sup>28,29</sup> mostly due to the lack of efficient synthetic strategies.

In this work, we report an efficient synthetic strategy toward three unprecedented sulfur-doped NGs containing two (1), six (2), and four (3) helicene substructures based on the well-

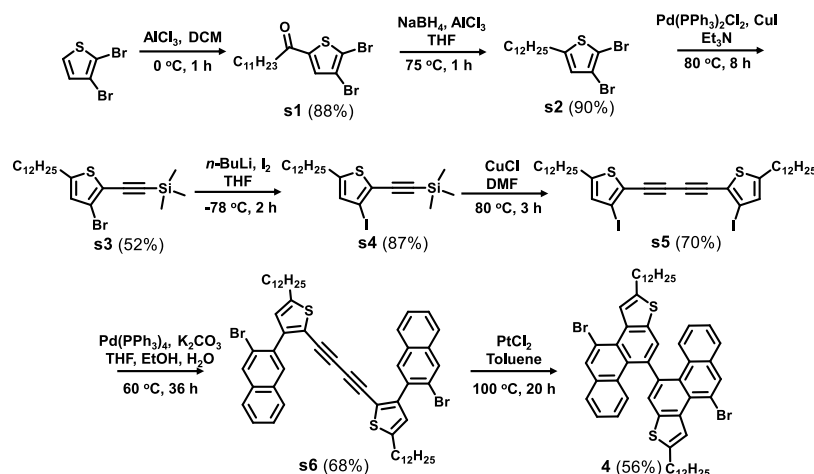
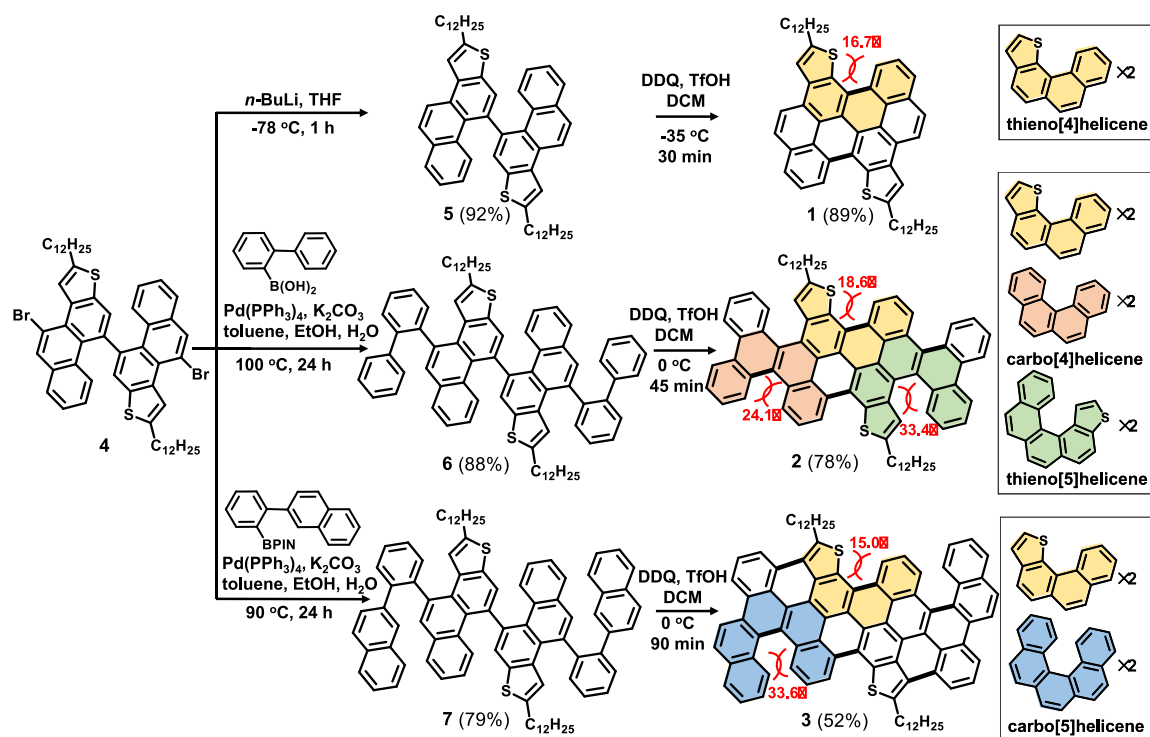


**Figure 1.** Structures of (a) representative multiple helicenes and (b) sulfur-doped NGs (1–3) with multiple helicene substructures reported in this work, including carbo[4]helicenes (orange), thieno[4]helicenes (yellow), carbo[5]helicenes (blue), and thieno[5]helicenes (green).

Received: January 21, 2021

Published: March 2, 2021

Scheme 1. Illustration of the Synthesis of Key Building Block 4

Scheme 2. Illustration of the Synthesis of NGs 1–3<sup>a</sup>

<sup>a</sup>The dihedral angles were calculated at the B3LYP/6-31G(d) level.

controlled cyclodehydrogenation reactions (Figure 1b). Compound 1 consists of a pair of thieno[4]helicenes (yellow). Further lateral extension of 1 by fusing two phenanthrene units, compound 2 bearing additional two pairs of carbo[4]helicenes (orange) and thieno[5]helicenes (green), was achieved. Compound 3 containing an extra pair of carbo[5]helicenes (blue) was subsequently synthesized by fusing two chrysene moieties into 1. Density functional theory (DFT) calculations revealed that the helicene substructures in 1–3 possess dihedral angles of 15–34°, which are responsible for the excellent solubility of these NGs. The aromaticity of the resultant NGs was evaluated to be aromatic character by calculations. This study opens a new avenue for the precise synthesis of novel nonplanar NGs and also offers new insight into the

contributions of sulfur doping and helicene substructures to the physicochemical properties of NGs.

The synthetic routes toward 1–3 are illustrated in Schemes 1 and 2. First, the key building block 4,4'-dibromo-2,2'-didodecyl-10,10'-biphenanthro[2,1-*b*]thiophene (4) was synthesized as depicted in Scheme 1. Compound 2,3-dibromo-5-dodecylthiophene (s2) was obtained by Friedel–Crafts acylation and carbonyl reduction in 88 and 90% yields, respectively. Afterward, a selective Sonogashira reaction of s2 with trimethylsilylacetylene afforded [(3-bromo-5-dodecylthiophen-2-yl)ethynyl]trimethylsilane (s3) in 52% yield. Then, the bromo groups were transformed into iodo groups, affording [(5-dodecyl-3-iodothiophen-2-yl)ethynyl]trimethylsilane (s4) in 87% yield. Glaser self-coupling of s4 provided 1,4-bis(5-dodecyl-3-iodothiophen-2-yl)buta-1,3-diyne (s5) in 70% yield.

Subsequently, 1,4-bis[3-(3-bromonaphthalen-2-yl)-5-dodecylthiophen-2-yl]buta-1,3-diyne (**s6**) was furnished through the Suzuki coupling of **s5** and 2-bromo-3-naphthaleneboronic acid in 68% yield. Then the Pt-induced cyclization of **s6** afforded compound **4** in 56% yield (see details in the Supporting Information).

The key intermediate compound **4** was subsequently subjected to the synthesis of precursor compounds for the final sulfur-doped NGs (Scheme 2). Treatment of **4** with *n*-butyllithium gave 2,2'-didodecyl-10,10'-biphenanthro[2,1-*b*]thiophene (**5**) in 92% yield. The 2-fold Suzuki coupling of **4** afforded 4,4'-di([1,1'-biphenyl]-2-yl)-2,2'-didodecyl-10,10'-biphenanthro[2,1-*b*]thiophene (**6**) and 2,2'-didodecyl-4,4'-bis[2-(naphthalen-2-yl)phenyl]-10,10'-biphenanthro[2,1-*b*]thiophene (**7**) in 88% and 79% yields, respectively (Scheme 2). Finally, the well-controlled Scholl reactions allowed the formation of **1–3** containing multiple subhelicenes with good yields, including double, hexuple, and quadruple helicenes, respectively (Scheme 2). Compound **1** was achieved from **5** in 89% yield by fusing two C–C bonds, leading to the formation of a pair of thieno[4]helicenes. Compound **2** was synthesized from **6** in 78% yield via the cyclization of four C–C bonds, resulting in two additional pairs of carbo[4]helicenes and thieno[5]helicenes. Compound **3** was obtained from **7** in 52% yield, in which six C–C bonds were fused and an extra pair of carbo[5]helicenes was generated accordingly. Interestingly, compound **3** fused two more C–C bonds than **2** during the cyclodehydrogenation. This is likely due to the different distance between the thiophene ring and opposite benzene ring in their precursors **6** and **7**, which is driven by their respective steric hindrance. All targeted compounds (**1–3**) were purified by preparative thin-layer chromatography and then recrystallized from dichloromethane (DCM) and methanol. The chemical identities of targeted compounds **1–3** were confirmed by <sup>1</sup>H and <sup>13</sup>C NMR spectroscopy (one- and two-dimensional) as well as high-resolution mass spectrometry (Figures S1–S20).

On the basis of the DFT [B3LYP/6-31G(d)] calculations, the dihedral angles of different helicene substructures were examined. Among them, the dihedral angle of thieno[4]helicene in **1** (Scheme 2, yellow) was predicted to be ~16.7°, which is smaller than that of the pristine carbon analogue [4]helicene (~37°)<sup>16</sup> due to the weakened steric interactions by the introduction of thiophene rings. Likewise, **2** and **3** were estimated to have similar angles of 18.6° and 15.0°, respectively, at the same cove position. The dihedral angle of thieno[5]helicenes in **2** (Scheme 2, green) was calculated to be 33.4°, which is similar to that of carbo[5]helicenes in **3** (Scheme 2, blue). The carbo[4]helicenes in **2** (Scheme 2, orange) showed a dihedral angle of 24.1°, smaller than that of the carbon analogue [4]helicene (~37°), which is probably affected by the adjacent thieno[4]helicenes. Because of the multiple helicene substructures and the corresponding curvatures, compounds **1–3** have good solubility in common organic solvents, such as DCM, THF, toluene, etc.

The existence of different helicene substructures results in multiple chirality centers and thus a variety of possible isomers for **1–3**. While different atropisomers were observed for precursors **6** and **7** (for rates and energies see chapter 4 of the Supporting Information), the <sup>1</sup>H NMR spectra of **1** and **3** showed well-resolved signals at room temperature (Figure 2 and Figures S4 and S14). For **1**, a residual line broadening disappears at a slightly increased temperature (Figure S5),

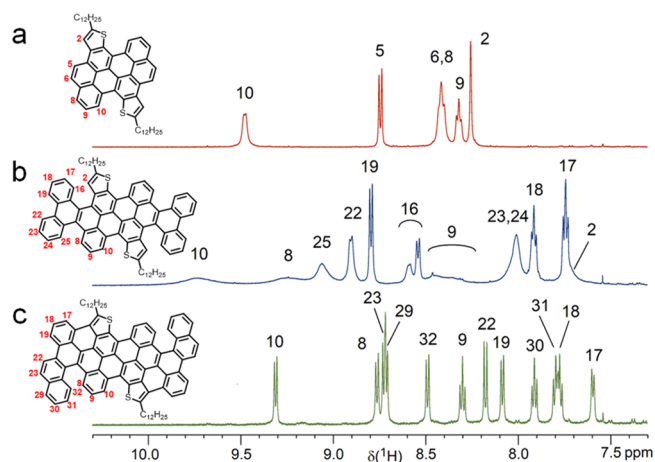


**Figure 2.** <sup>1</sup>H NMR spectra (aromatic region) of (a) **1**, (b) **2**, and (c) **3** in dichloromethane-*d*<sub>2</sub> at 30 °C.

which is attributed to the inversion of thieno[4]helicenes. The additional ring fusion of the thienyl moiety results in flattened thieno[4]helicenes in **3** compared to **1** [15.0° vs 16.7° (Scheme 2)]. Therefore, a faster interconversion is expected, which results in the observed narrow signals for **3** in the temperature range from 30 to 120 °C (Figure S20). Compound **2** combines six subhelicenes with three different types of helicene substructures. The <sup>1</sup>H NMR spectrum of **2** is clearly influenced by the dynamic processes (Figure 2b), which were observed over the whole temperature range studied [−30 to 120 °C (Figure S11)]. It can be assumed that the additional carbo[4]helicenes (with a dihedral angle of 24.1°) are the main cause of line broadening in the NMR spectra of **2**, which is also supported by the broadened signals of H<sub>24</sub> and H<sub>25</sub> (Figure 2b). The effect is most pronounced for H<sub>8</sub>–H<sub>10</sub>, which are involved in the carbo[4]helicene and thieno[4]helicene motions. The fixed helicity of the thieno[5]helicenes in **2** is indicated by signals of two isomers for H<sub>16</sub> with an almost constant ratio and rather narrow signals for H<sub>16</sub>–H<sub>19</sub>, which narrow further with an increase in temperature (Figure S11). The complex overall dynamic process of **2** stands for its multilevel helicene substructures in which all individual motions seem to interlock.<sup>30</sup>

The UV–vis absorption spectra of **1–3** in anhydrous DCM solutions are presented in Figure 3a. The spectrum of **1** exhibited a maximum absorption peak ( $\lambda_{\text{max}}$ ) at 449 nm and an absorption onset at 465 nm, corresponding to an optical energy gap of 2.67 eV. In comparison with the reported pristine carbon analogue of **1** [A (Figure 1a)],<sup>16</sup> which showed a maximum absorption of 502 nm and an optical energy gap of 2.36 eV, sulfur-doped **1** exhibited an enlarged energy gap. The similar tendency was also found for both **2** and **3** based on the calculation results (Figure S41), compared with their respective carbon analogues. Due to the extended  $\pi$ -conjugation, both **2** and **3** displayed obvious red-shifted absorption peaks compared to **1**, with  $\lambda_{\text{max}}$  values of 485 and 500 nm. The optical energy gaps of **2** and **3** are estimated to be 2.45 and 2.30 eV, respectively. Compounds **1–3** exhibited blue, green, and orange fluorescence, respectively, and their maximum emission peaks were observed at 460, 505, and 569 nm, respectively (Figure 3a, dashed lines). Interestingly, compound **2** containing three types of subhelicenes exhibited an absolute quantum yield of 13.8%, higher than those of **1** (4.5%) and **3** (3.8%). The electrochemical behaviors of **1–3** were investigated by cyclic

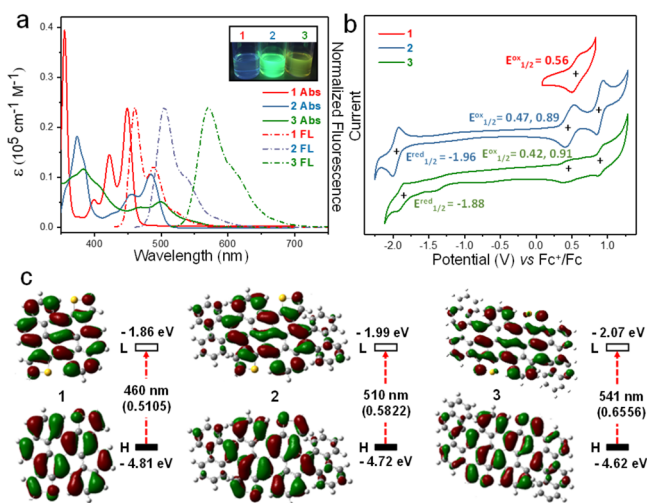


**Figure 3.** (a) UV-vis absorption spectra (solid lines) and fluorescence spectra (dashed lines) of 1–3 in DCM ( $10^{-5}$  M). The inset shows the photograph of 1–3 under emission. (b) Cyclic voltammograms of 1–3 in DCM containing 0.1 M *n*-Bu<sub>4</sub>NPF<sub>6</sub> at a scan rate of 0.1 V s<sup>-1</sup>. Ferrocene was used as an external standard. (c) Molecular orbitals and their energy diagrams calculated at the B3LYP/6-31G(d) level of 1–3. Values in brackets represent the oscillator strengths (*f*). H, HOMO; L, LUMO.

voltammetry (CV) in anhydrous DCM. As illustrated in Figure 3b, compound 1 featured one reversible oxidation wave with a half-wave potential  $E_{1/2}^{\text{ox}}$  of 0.56 V (vs Fc<sup>+</sup>/Fc) and did not show any reduction process in the cathodic potential range. However, compound 2 displayed two reversible oxidation waves with  $E_{1/2}^{\text{ox}}$  values at 0.47 and 0.89 V, and one reversible reduction wave with an  $E_{1/2}^{\text{red}}$  at -1.96 V. In addition, 3 exhibited two reversible oxidation waves with  $E_{1/2}^{\text{ox}}$  values at 0.42 and 0.91 V, and one reversible reduction wave with an  $E_{1/2}^{\text{red}}$  at -1.88 V. Accordingly, the highest occupied molecular orbital (HOMO)/lowest unoccupied molecular orbital (LUMO) levels were estimated to be -5.29, -5.16/-2.93, and -5.15/-3.03 eV for 1–3, respectively, based on the onset potentials of the first oxidation/reduction waves. The electrochemical energy gaps ( $E_{\text{g,CV}}$ ) were thus calculated to be 2.23 and 2.12 eV for 2 and 3, respectively, which are in good accordance with their optical energy gaps.

To gain deeper insight into their electronic structures, DFT calculations at the B3LYP/6-31G(d) level were performed (Figure 3c). For 1, both the HOMO and LUMO were delocalized over the entire conjugated backbone. The  $\pi$ -extension of 2 and 3 leads to an enlarged electron delocalization over the whole molecular skeleton. The calculated HOMO and LUMO energy levels as well as energy gaps are summarized in Table S1. Moreover, according to the time-dependent (TD)-DFT calculations, the maximum absorption peaks of 1 (calculated value of 460 nm), 2 (calculated value of 510 nm), and 3 (calculated value of 541 nm) can be assigned to the HOMO  $\rightarrow$  LUMO transition, which are in good agreement with the experimentally measured results (Table S1).

The nucleus-independent chemical shift (NICS) calculations (Figure 4) were conducted to evaluate the aromaticity of compounds 1–3. The dodecyl groups in 1–3 were replaced with methyl groups to simplify the calculations (namely 1'–3', respectively). The NICS(1)<sub>zz</sub> values of most of rings in 1'–3' are negative, showing the aromatic character. On the contrary, ring a in 3' shows a positive NICS(1)<sub>zz</sub> value of 10.5, indicating

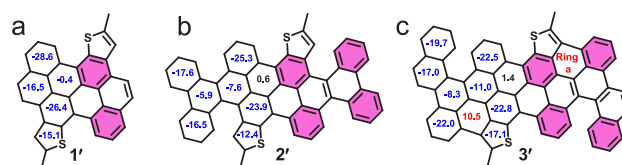


**Figure 4.** NICS(1)<sub>zz</sub> values (in parts per million) of (a) 1', (b) 2', and (c) 3' calculated at the GIAO-B3LYP/6-311+G(2d,p) level.

its antiaromatic character. According to the NICS calculations, compounds 1–3 exhibit aromatic character, in line with their resonance structures (Figure 4, highlighted in pink).

In summary, we demonstrated the novel synthesis of a series of sulfur-doped NGs with multiple helicene substructures. DFT calculations revealed that the subhelicenes in these NGs possess the dihedral angles from 15° to 34°. Compared to the pristine carbon analogues, sulfur-doped NGs showed enlarged energy gaps. These novel sulfur-doped curved NGs hold promise in the applications of optoelectronic devices, and the synthetic strategy described herein can be further extended to synthesize structurally well-defined sulfur-doped graphene nanoribbons.

## ■ ASSOCIATED CONTENT

### Supporting Information

The Supporting Information is available free of charge at <https://pubs.acs.org/doi/10.1021/acs.orglett.1c00232>.

Experimental details, supporting figures, and calculations (PDF)

## ■ AUTHOR INFORMATION

### Corresponding Authors

**Yiyong Mai** – School of Chemistry and Chemical Engineering, Frontiers Science Center for Transformative Molecules, Shanghai Key Laboratory of Electrical Insulation and Thermal Ageing, Shanghai Jiao Tong University, Shanghai 200240, China; [orcid.org/0000-0002-6373-2597](https://orcid.org/0000-0002-6373-2597); Email: [mai@sjtu.edu.cn](mailto:mai@sjtu.edu.cn)

**Junzhi Liu** – Department of Chemistry and State Key Laboratory of Synthetic Chemistry, The University of Hong Kong, Hong Kong 999077, China; [orcid.org/0000-0001-7146-0942](https://orcid.org/0000-0001-7146-0942); Email: [juliu@hku.hk](mailto:juliu@hku.hk)

### Authors

**Wenhui Niu** – School of Chemistry and Chemical Engineering, Frontiers Science Center for Transformative Molecules, Shanghai Key Laboratory of Electrical Insulation and Thermal Ageing, Shanghai Jiao Tong University, Shanghai 200240, China; Center for Advancing Electronics Dresden (cfaed) and Faculty of Chemistry and Food Chemistry, Technische Universität Dresden, D-01062 Dresden, Germany; [orcid.org/0000-0003-4003-5550](https://orcid.org/0000-0003-4003-5550)

**Yubin Fu** – Center for Advancing Electronics Dresden (cfaed) and Faculty of Chemistry and Food Chemistry, Technische Universität Dresden, D-01062 Dresden, Germany; [orcid.org/0000-0002-2613-394X](https://orcid.org/0000-0002-2613-394X)

**Hartmut Komber** – Leibniz-Institut für Polymerforschung Dresden e. V., D-01069 Dresden, Germany; [orcid.org/0000-0001-6176-6737](https://orcid.org/0000-0001-6176-6737)

**Ji Ma** – Center for Advancing Electronics Dresden (cfaed) and Faculty of Chemistry and Food Chemistry, Technische Universität Dresden, D-01062 Dresden, Germany; [orcid.org/0000-0003-4418-2339](https://orcid.org/0000-0003-4418-2339)

Xinliang Feng – Center for Advancing Electronics Dresden (cfaed) and Faculty of Chemistry and Food Chemistry, Technische Universität Dresden, D-01062 Dresden, Germany; [orcid.org/0000-0003-3885-2703](https://orcid.org/0000-0003-3885-2703)

Complete contact information is available at:  
<https://pubs.acs.org/10.1021/acs.orglett.1c00232>

## Notes

The authors declare no competing financial interest.

## ACKNOWLEDGMENTS

Y.M. is grateful for the financial support from the National Natural Science Foundation of China (21774076 and 52073173), the Program of Shanghai Academic Research Leader (19XD1421700), and the Program of Distinguished Professor of Special Appointment at Shanghai Institutions of Higher Learning. X.F. thanks the European Union's Horizon 2020 (881603 Graphene Flagship Core3, 813036 Marie Skłodowska-Curie), ERC Grant on T2DCP, German DFG [Cluster of Excellence "Center for Advancing Electronics Dresden (cfaed)"], and DFG NSFC Joint Sino-German Research Project (EnhanceNano), as well as the DFG-SNSF Joint Switzerland-German Research Project (EnhanTopo). J.L. is grateful for the Hong Kong Research Grants Council (HKU 27301720) and the funding support from ITC to the SKL. The authors are grateful for the assistance of F. Drescher and Prof. E. Brunner for the HR-MS measurements. The authors also appreciate the Instrumental Analysis Center at Shanghai Jiao Tong University for some analyses. The authors thank the Center for Information Services and High Performance Computing (ZIH) at TU Dresden for generous allocations of compute resources.

## REFERENCES

- (1) Pun, S. H.; Miao, Q. Toward Negatively Curved Carbons. *Acc. Chem. Res.* **2018**, *51*, 1630–1642.
- (2) Kawasumi, K.; Zhang, Q.; Segawa, Y.; Scott, L. T.; Itami, K. A grossly warped nanographene and the consequences of multiple odd-membered-ring defects. *Nat. Chem.* **2013**, *5*, 739–744.
- (3) Ball, M.; Zhong, Y.; Wu, Y.; Schenck, C.; Ng, F.; Steigerwald, M.; Xiao, S.; Nuckolls, C. Contorted Polycyclic Aromatics. *Acc. Chem. Res.* **2015**, *48*, 267–276.
- (4) Zhu, Y.; Xia, Z.; Cai, Z.; Yuan, Z.; Jiang, N.; Li, T.; Wang, Y.; Guo, X.; Li, Z.; Ma, S.; Zhong, D.; Li, Y.; Wang, J. Synthesis and Characterization of Hexapole [7]Helicene, A Circularly Twisted Chiral Nanographene. *J. Am. Chem. Soc.* **2018**, *140*, 4222–4226.
- (5) Wang, Y.; Yin, Z.; Zhu, Y.; Gu, J.; Li, Y.; Wang, J. Hexapole [9]Helicene. *Angew. Chem., Int. Ed.* **2019**, *58*, 587–591.
- (6) Fernández-García, J. M.; Evans, P. J.; Filippone, S.; Herranz, M. Á.; Martín, N. Chiral Molecular Carbon Nanostructures. *Acc. Chem. Res.* **2019**, *52*, 1565–1574.
- (7) Naaman, R.; Waldeck, D. H. Chiral-Induced Spin Selectivity Effect. *J. Phys. Chem. Lett.* **2012**, *3*, 2178–2187.
- (8) Gingras, M. One hundred years of helicene chemistry. Part 3: applications and properties of carbohelicenes. *Chem. Soc. Rev.* **2013**, *42*, 1051–1095.
- (9) Rickhaus, M.; Mayor, M.; Juriček, M. Strain-induced helical chirality in polyaromatic systems. *Chem. Soc. Rev.* **2016**, *45*, 1542–1556.
- (10) Shen, Y.; Chen, C.-F. Helicenes: Synthesis and Applications. *Chem. Rev.* **2012**, *112*, 1463–1535.
- (11) Ogawa, N.; Yamaoka, Y.; Takikawa, H.; Yamada, K.-i.; Takasu, K. Helical Nanographenes Embedded with Contiguous Azulene Units. *J. Am. Chem. Soc.* **2020**, *142*, 13322–13327.
- (12) Ma, J.; Fu, Y.; Dmitrieva, E.; Liu, F.; Komber, H.; Hennersdorf, F.; Popov, A. A.; Weigand, J. J.; Liu, J.; Feng, X. Helical Nanographenes Containing an Azulene Unit: Synthesis, Crystal Structures, and Properties. *Angew. Chem., Int. Ed.* **2020**, *59*, 5637–5642.
- (13) Nakakuki, Y.; Hirose, T.; Sotome, H.; Miyasaka, H.; Matsuda, K. Hexa-peri-hexabenz[7]helicene: Homogeneously  $\pi$ -Extended Helicene as a Primary Substructure of Helically Twisted Chiral Graphenes. *J. Am. Chem. Soc.* **2018**, *140*, 4317–4326.
- (14) Fujikawa, T.; Preda, D. V.; Segawa, Y.; Itami, K.; Scott, L. T. Corannulene–Helicene Hybrids: Chiral  $\pi$ -Systems Comprising Both Bowl and Helical Motifs. *Org. Lett.* **2016**, *18*, 3992–3995.
- (15) Fernández-García, J. M.; Evans, P. J.; Medina Rivero, S.; Fernández, I.; García-Fresnadillo, D.; Perles, J.; Casado, J.; Martín, N.  $\pi$ -Extended Corannulene-Based Nanographenes: Selective Formation of Negative Curvature. *J. Am. Chem. Soc.* **2018**, *140*, 17188–17196.
- (16) Liu, J.; Li, B.-W.; Tan, Y.-Z.; Giannakopoulos, A.; Sanchez-Sanchez, C.; Beljonne, D.; Ruffieux, P.; Fasel, R.; Feng, X.; Müllen, K. Toward Cove-Edged Low Band Gap Graphene Nanoribbons. *J. Am. Chem. Soc.* **2015**, *137*, 6097–6103.
- (17) Kashihara, H.; Asada, T.; Kamikawa, K. Synthesis of a Double Helicene by a Palladium-Catalyzed Cross-Coupling Reaction: Structure and Physical Properties. *Chem. - Eur. J.* **2015**, *21*, 6523–6527.
- (18) Zhang, F.; Michail, E.; Saal, F.; Krause, A.-M.; Ravat, P. Stereospecific Synthesis and Photophysical Properties of Propeller-Shaped  $C_{90}H_{48}$  PAH. *Chem. - Eur. J.* **2019**, *25*, 16241–16245.
- (19) Li, C.; Yang, Y.; Miao, Q. Recent Progress in Chemistry of Multiple Helicenes. *Chem. - Asian J.* **2018**, *13*, 884–894.
- (20) Mori, T. Chiroptical Properties of Symmetric Double, Triple, and Multiple Helicenes. *Chem. Rev.* **2021**, *121*, 2373–2412.
- (21) Wang, X.-Y.; Yao, X.; Narita, A.; Müllen, K. Heteroatom-Doped Nanographenes with Structural Precision. *Acc. Chem. Res.* **2019**, *52*, 2491–2505.
- (22) Narita, A.; Wang, X.-Y.; Feng, X.; Müllen, K. New advances in nanographene chemistry. *Chem. Soc. Rev.* **2015**, *44*, 6616–6643.
- (23) Liu, J.; Feng, X. Bottom-Up Synthesis of Nitrogen-Doped Polycyclic Aromatic Hydrocarbons. *Synlett* **2020**, *31*, 211–222.
- (24) Stępień, M.; Gońka, E.; Żyła, M.; Sprutta, N. Heterocyclic Nanographenes and Other Polycyclic Heteroaromatic Compounds: Synthetic Routes, Properties, and Applications. *Chem. Rev.* **2017**, *117*, 3479–3716.
- (25) Xu, K.; Fu, Y.; Zhou, Y.; Hennersdorf, F.; Machata, P.; Vincon, I.; Weigand, J. J.; Popov, A. A.; Berger, R.; Feng, X. Cationic Nitrogen-Doped Helical Nanographenes. *Angew. Chem., Int. Ed.* **2017**, *56*, 15876–15881.
- (26) Chen, L.; Mali, K. S.; Puniredd, S. R.; Baumgarten, M.; Parvez, K.; Pisula, W.; De Feyter, S.; Müllen, K. Assembly and Fiber Formation of a Gemini-Type Hexathienocoronene Amphiphile for Electrical Conduction. *J. Am. Chem. Soc.* **2013**, *135*, 13531–13537.
- (27) Chen, L.; Puniredd, S. R.; Tan, Y.-Z.; Baumgarten, M.; Zschieschang, U.; Enkelmann, V.; Pisula, W.; Feng, X.; Klauk, H.; Müllen, K. Hexathienocoronenes: Synthesis and Self-Organization. *J. Am. Chem. Soc.* **2012**, *134*, 17869–17872.
- (28) Chiu, C.-Y.; Kim, B.; Gorodetsky, A. A.; Sattler, W.; Wei, S.; Sattler, A.; Steigerwald, M.; Nuckolls, C. Shape-shifting in contorted dibenzotetrathienocoronenes. *Chem. Sci.* **2011**, *2*, 1480–1486.
- (29) Fujikawa, T.; Segawa, Y.; Itami, K. Synthesis and Structural Features of Quadruple Helicenes: Highly Distorted  $\pi$  Systems Enabled by Accumulation of Helical Repulsions. *J. Am. Chem. Soc.* **2016**, *138*, 3587–3595.
- (30) Hosokawa, T.; Takahashi, Y.; Matsushima, T.; Watanabe, S.; Kikkawa, S.; Azumaya, I.; Tsurusaki, A.; Kamikawa, K. Synthesis, Structures, and Properties of Hexapole Helicenes: Assembling Six [5]Helicene Substructures into Highly Twisted Aromatic Systems. *J. Am. Chem. Soc.* **2017**, *139*, 18512–18521.